Mon. Not. R. Astron. Soc. **000**, 1–17 (2007) Printed 19 September 2008 (MN LATEX style file v2.2)

The impact of Early Dark Energy on non-linear structure formation

Margherita Grossi[1], Volker Springel[1]
[1] *Max-Planck Institut fuer Astrophysik, Karl-Schwarzschild Strasse 1, D-85748 Garching, Germany*
(margot@mpa-garching.mpg.de),(volker@mpa-garching.mpg.de)

Accepted ???. Received ???; in original form

ABSTRACT

We study non-linear structure formation in high-resolution simulations of Early Dark Energy (EDE) cosmologies and compare their evolution with the standard ΛCDM model. In Early Dark Energy models, the impact on structure formation is expected to be particularly strong because of the presence of a non-negligible dark energy component even at very high redshift, unlike in standard models that behave like matter-dominated universes at early times. In fact, extensions of the spherical top-hat collapse model predict that the virial overdensity and linear threshold density for collapse should be modified in EDE model, yielding significant modifications in the expected halo mass function. Here we present numerical simulations that directly test these expectations. Interestingly, we find that the Sheth & Tormen formalism for estimating the abundance of dark matter halos continues to work very well in its standard form for the Early Dark Energy cosmologies, contrary to analytic predictions. The residuals are even slightly smaller than for ΛCDM. We also study the virial relationship between mass and dark matter velocity dispersion in different dark energy cosmologies, finding excellent agreement with the normalization for ΛCDM as calibrated by Evrard et al. (2008). The earlier growth of structure in EDE models relative to ΛCDM produces large differences in the mass functions at high redshift. This could be measured directly by counting groups as a function of the line-of-sight velocity dispersion, skirting the ambiguous problem of assigning a mass to the halo. Using dark matter substructures as a proxy for member galaxies, we demonstrate that even with 3-5 members sufficiently accurate measurements of the halo velocity dispersion function are possible. Finally, we determine the concentration-mass relationship for our EDE cosmologies. Consistent with the earlier formation time, the EDE halos show higher concentrations at a given halo mass. We find that the magnitude of the difference in concentration is well described by the prescription of Eke et al. (2001) for estimating halo concentrations.

Key words: early universe – cosmology: theory – galaxies: formation

1 INTRODUCTION

Arguably the most surprising result of modern cosmology is that all matter (including both atoms and non-baryonic dark matter) accounts for only a quarter of the total energy density of the Universe today, while the rest is contributed by a *dark energy* field. In 1999, observations of type Ia supernovae by the Supernovae Cosmology Project (Riess et al. 1999; Riess 2004) and the relative accurate measurements of the distances to this objects (Perlmutter 1999; Kowalski 2008) demonstrated that the expansion of the Universe is accelerated today; there hence exists a mysterious force that acts against the pull of gravity. Nowadays, the inference that this is caused by dark energy can be made with significant confidence, as the observational evidence has further firmed up. In fact, we have good reason to believe that we live in a flat universe with an upper limit of $\Omega_m \leqslant 0.3$ for the matter density today, based on cosmic microwave background measurements and a host of other observational probes (Komatsu et al. 2008, e.g.). These observations yield a consistent picture, the so-called concordance cosmology, and are in agreement with predictions of the inflationary theory.

The physical origin of dark energy is however unknown and a major puzzle for theoretical physics. A nagging outstanding problem is that most quantum field theories predict a huge cosmological constant from the energy of the quantum vacuum, up to 120 orders of magnitude too large. There is hence no simple natural explanation for dark energy, and one has to be content with phenomenological models at this point. Two proposed forms of dark energy are the cosmological constant, a constant energy density filling space homogeneously, and scalar fields such as quintessence. In particular, 'tracking quintessence' models attempt to alleviate the coincidence problem of the cosmological constant model. More exotic models where the dark energy couples to matter fields or can cluster itself have also been proposed.

In light of the many theoretical possibilities, the hope is that future observational constraints on dark energy will enable progress in the understanding of this puzzling phenomenon. This requires

the exploitation of the subtle influence of dark energy on structure formation, both on linear and non-linear scales. As the expected effects are generally small for many of the viable dark energy scenarios, it is crucial to be able to calculate structure formation in dark energy cosmologies with sufficient precision to tell the different models apart, and to be able to correctly interpret observational data. For example, in order to use the abundance of clusters of galaxies at different epochs to measure the expansion history of the universe, one needs to reliably know how the cluster mass function evolves with time in different dark energy cosmologies. Numerical simulations are the most accurate tool available to obtain the needed theoretical predictions, and they are also crucial for testing the results of more simplified analytic calculations.

In this study, we carry out such non-linear simulations for a particular class of dark energy cosmologies, so-called Early Dark Energy (EDE) models where dark energy might constitute an observable fraction of the total energy density of our Universe at the time of matter radiation equality or even big-bang nucleosynthesis. While in the cosmological constant scenario, the fraction in dark energy is negligible at high redshift, in such models the energy fraction is a few per cent during recombination and structure formation, which introduces interesting effects due to dark energy already at high redshift. In particular, for an equal amplitude of clustering today, we expect structures to form earlier in such cosmologies than in ΛCDM. This could be useful to alleviate the tension between a low σ_8 normalization suggested by current observational constraints from the CMB on one hand, and the observations of relatively early reionization and the existence of a population of massive halos present already at high redshift on the other hand.

Recently, Bartelmann et al. (2006) studied two particular EDE models, evaluating the primary quantities relevant for structure formation, such as the linear growth factor of density perturbation, the critical density for spherical collapse and the overdensity at virialization, and finally the halo mass function. In the two models analyzed, they found that the effect of EDE on the geometry of the Universe is only moderate, for example, distance measures can be reduced by 8%. Assuming the same expansion rate today, such models are younger compared to ΛCDM. At early times, the age of the universe should differ by approximately $5-10\%$.

However, when Bartelmann et al. (2006) repeated the calculation of the spherical collapse model in the EDE cosmology, a few nontrivial modifications appeared. The evolution of a homogeneous, spherical overdensity can be traced utilizing both the virial theorem and the energy conservation between the collapse and the turn around time (see also Lacey & Cole 1993; Wang & Steinhardt 1998). Bartelmann et al. (2006) obtained the value of the virial overdensity as a function of the collapse redshift, translating the effect of the early dark energy in an extra contribution to the potential energy at early times. They found that the virial overdensity should be slightly enlarged by EDE, because a faster expansion of the universe means that, by the time a perturbation has turned around and collapsed to its final radius, a larger density contrast has been produced. However, at the same time they found that the linearly extrapolated density contrast corresponding to the collapsed object should be significantly reduced.

These two results based on analytic expectations have a pronounced influence on the predicted mass function of dark matter halos. In EDE models, the cluster population expected from the Press-Schechter or Sheth-Tormen formalism grows considerably relative to ΛCDM, as a result of the lowered value of the critical linear density contrast δ_c for collapse. This effect can be compensated for by lowering the normalization parameter σ_8 in order to obtain the same abundance of clusters today. In this case, one would however still expect a higher cluster abundance in EDE at high redshift, due to the earlier growth of structure in this model.

An open question is whether the EDE really participates in the virialization process in the way assumed in the analytic modeling. Similarly, it is not clear whether the excursion set formalism of Sheth & Tormen yields an equally accurate description of the non-linear mass function of halos in EDE cosmologies as in ΛCDM. Because accurate theoretical predictions for the halo mass function are a critical ingredient for constraining cosmological parameters (in particular Ω_m and Ω_Λ) as well as models of galaxy formation, it is important to test these predictions for the EDE cosmology in detail with numerical N-body simulations. In particular, we want to probe whether the fraction f of matter ending up in objects larger than a given mass M at some redshift z can be found by *only* looking at the properties of the linearly evolved density field at this epoch, using the ordinary ST formalism, or whether there is some dependence on redshift, power spectrum or dark energy parameters, as suggested by Bartelmann et al. (2006).

A further interest in EDE cosmologies stems from the fact that for a given σ_8, the EDE models predict a substantially slower evolution of the halo population than in the ΛCDM model. This could explain the higher normalization cosmology expected from cluster studies relative to analysis of the CMB. The value of σ_8, for a given cosmology, provides also a measure of the expected biasing parameter that relates the galaxy and the mass distribution. The early dark energy cosmologies could hence reduce the current mild tension between cluster data and the CMB observations. We note that halos in cosmologies with EDE are also expected to be more concentrated than in ΛCDM; because the density of the Universe was greater at early times, objects that virialized at high redshift are more compact than those that virialized more recently.

Previous numerical simulations of a quintessence component with a changing equation of state (EOS) explored two particular potentials: SUGRA and Ratra Peebles (RP), which differ because RP has a more smoothly decreasing w and consequently a very different evolution in the past. Both Linder & Jenkins (2003) and Klypin et al. (2003) analyzed the influence of the dark energy on the halo mass function in order to extrapolate the abundance of structure at different epochs and to compare it with existent theoretical models. They used different numerical codes: the publicly available code GADGET, in the first project, and the Adaptive Refinement Tree code (Kravtsov et al. 1997), in the second. They concluded that the best way to understand which dark energy Universe fit the observations best is to look at the growth history of halos and the evolution of their properties with time. Dolag et al. (2004) focused on the modification of the concentration parameter with mass and redshift, for the same cosmologies, based on high resolution simulations of a sample of massive halos. A limited number of numerical studies also considered the possibility of a coupling of the dark energy field with dark matter (Mainini et al. 2003; Macciò et al. 2004).

In this paper, we carry out several high resolution simulations of dark energy cosmologies in order to accurately measure the quantitative impact of early dark energy on abundance and structure of dark matter halos. To this end, we in particular measure halo mass functions and evaluate the agreement/disagreement with different analytic fitting functions. We also test how well the growth of the mass function can be tracked with dynamical measure based on the velocity dispersion of dark matter substructures, which can serve as a proxy for the directly measurable line-of-sight motion of galaxies or line widths in observations, and gets around the usual

ambiguities arising from different possible mass definitions for halos. Finally, we also present measurements of halo concentrations, and of the relation between dark matter velocity dispersion and halo mass. While finalizing this paper, Francis et al. (2008) submitted a preprint which also studies numerical simulations of EDE cosmologies. Their work provides a different analysis and is complementary to our study, but it reaches similar basic conclusions about the halo mass function.

This paper is organized as follows. After a brief introduction to the Early Dark Energy models in Section 2, we present the simulations and also give details on our numerical methods in Section 3. In Section 4, we study the mass function of halos for the different cosmologies, and as a function of redshift. Then, in Section 5 we investigate the properties of halos by studying the virial relation between mass and dark matter velocity dispersion, as well as the mass–concentration relationship. In Section 6, we consider the velocity distribution function and prospects for measuring it in observations. Finally, we discuss our results and present our conclusions in Section 7.

2 EARLY DARK ENERGY MODELS

The influence of dark energy on the evolution of the Universe is governed by its equation of state,

$$p = w\rho c^2. \tag{1}$$

A cosmological constant has $w_\Lambda = -1$ at all redshift, while a distinctive feature of the Early Dark Energy (hereafter EDE) models as well as of other models such as quintessence is that their equation of state parameter, $w_{\rm de}(z)$, varies during cosmic history.

Negative pressure at all times implies that the energy density parameter will fall to zero very steeply for increasing redshift. If, however, we allow the equation of state parameter to rise above zero, we can construct models in which $\Omega_{\rm de}(z)$ has a small positive value at all epochs, depending on the cosmological background model we adopt. While canonical dark energy models with near constant behaviour for w do not predict any substantial dark energy effect at $z > 2$, in such EDE models the contribution of dark energy to the cosmic density can be of order of a few percent even at very high redshift.

We are here investigating this interesting class of models which are characterized by a low but non-vanishing dark energy density at early times. Note that while the acceleration of the expansion of the Universe is a quite recent phenomenon, the dark energy responsible for this process could have an old origin. In fact, field theoretical models have been constructed that generically cause such a dynamical behaviour (Ratra & Peebles 1988; Wetterich 1988; Ferreira & Joyce 1998; Liddle & Scherrer 1999).

Wetterich (2004) proposed a useful parameterization of a family of cosmological models with EDE in terms of three parameters:

- the amount of dark energy today, $\Omega_{\rm de,0}$ (we assume a flat universe, so $\Omega_{m,0} = 1 - \Omega_{\rm de,0}$),
- the equation-of-state parameter w_0 today, and
- an average value $\Omega_{\rm de,e}$ of the energy density parameter at early times (to which it asymptotes for $z \mapsto \infty$).

Figure 1 shows the redshift evolution of the equation-of-state parameter in the four different cosmologies that we examine in this study. As can be noticed, the EDE models approach the cosmological constant scenario at very low redshift. We can compute

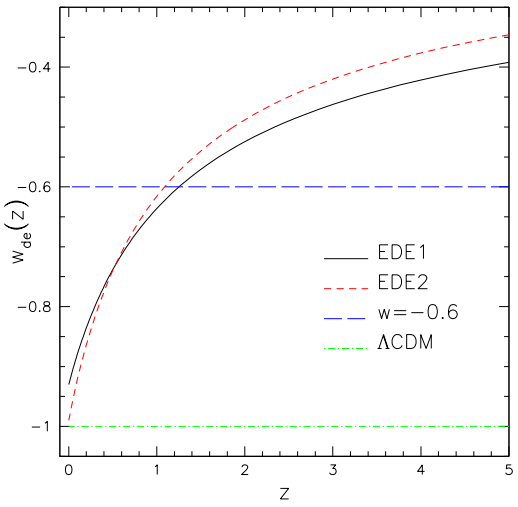

Figure 1. Equation of state parameter w shown as a function of redshift for the four different cosmological models considered in this work. In the two early dark energy models EDE1 and EDE2, shown with black solid and red dotted lines respectively, the value of w today is close to that of ΛCDM, but the amount of dark energy at early times is non vanishing, as described by the parameterization (2).

the equation-of-state parameter for these early dark energy models from the fitting formula:

$$w(z) = \frac{w_0}{(1+by)^2}, \tag{2}$$

where

$$b = -\frac{3w_0}{\ln\left(\frac{1/\Omega_{\rm de,e}}{\Omega_{\rm de,e}}\right) + \ln\left(\frac{1-\Omega_{m,0}}{\Omega_{m,0}}\right)}, \tag{3}$$

and $y = \ln(1+z) = -\ln a$. The parameter b characterizes the time at which an approximately constant equation-of-state changes its behaviour.

In Figure 2, we plot the evolution of the matter and energy density parameters up to redshift $z = 30$. The dark energy parameter for EDE models evolves relatively slowly with respect to a standard ΛCDM cosmology. In fact, the critical feature of this parameterization is a non-vanishing dark energy contribution during recombination and structure formation (see also Doran et al. 2001):

$$\bar{\Omega}_{\rm de,sf} = -\ln a_{\rm eq}^{-1} \int_{\ln a_{\rm eq}}^{0} \Omega_{\rm de}(a)\, {\rm d}\ln a. \tag{4}$$

For sufficiently low $\Omega_{\rm de,e}$, the EDE models reproduce quite well the accelerated cosmic expansion in the present-day Universe and they can be fine-tuned to agree both with low-redshift observations and CMB temperature fluctuation results (Doran et al. 2005, 2007).

3 NUMERICAL SIMULATIONS

We performed a series of cosmological N-body simulations for two early dark energy models 'EDE1' and 'EDE2', which have $w_0 = -0.93$ and $w_0 = -0.99$, respectively, and a dark energy density at early times of about 10^{-4} (see Tab. 1). For comparison, we have also calculated a model 'DECDM' with constant equation of state parameter equal to $w = -0.6$, and a conventional ΛCDM

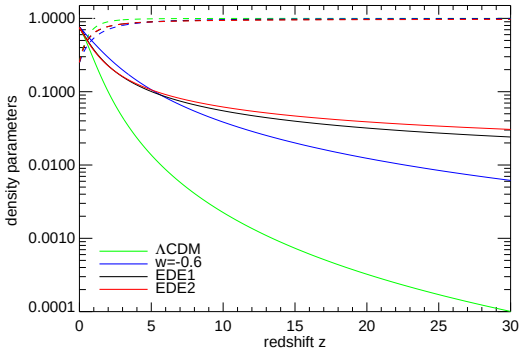

Figure 2. Evolution of the density parameters $\Omega_m(z)$ (dashed lines) and $\Omega_{\rm de}(z)$ (solid line) for the four cosmological models studied in this work. At redshift $z = 30$, the dark energy contribution is orders of magnitude higher for EDE models compared with a ΛCDM cosmology.

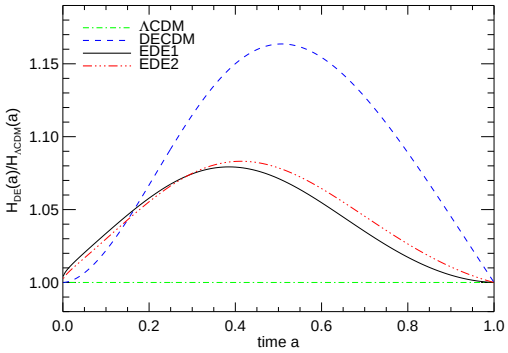

Figure 3. Hubble expansion rate for the models studied in this work. All models are normalized with respect to the reference ΛCDM case. In the models EDE1, EDE2, and in the model with constant w, the expansion rate of the universe is higher at early times. This has a strong effect on the evolution of the growth factor.

	$\Omega_{m,0}$	$\Omega_{\rm de,0}$	h_0	σ_8	w_0	$\Omega_{\rm de,e}$
ΛCDM	0.25	0.75	0.7	0.8	-1.	0.
DECDM	0.25	0.75	0.7	0.8	-0.6	0.
EDE1	0.25	0.75	0.7	0.8	-0.93	2×10^{-4}
EDE2	0.25	0.75	0.7	0.8	-0.99	8×10^{-4}

Table 1. Parameters of the N-Body simulations. The parameter $\Omega_{\rm de,e}$ describes the amount of dark energy at early times, see equation (3). This value, together with w_0, the value of the equation state parameter today, and $\Omega_{\rm de,0}$, the amount of dark energy today, completely describes our EDE models.

reference model. We shall refer with these labels to the different models throughout the paper.

In all our models, the matter density parameter today was chosen as $\Omega_m = 0.25$, and we consider a flat universe. The Hubble parameter is $h = H_0/(100\,{\rm km\,s^{-1}Mpc^{-1}}) = 0.7$ and we assume Gaussian density fluctuations with a scale-invariant primordial power spectrum. The normalization of the linear power spectrum extrapolated to $z = 0$ is $\sigma_8 = 0.8$ for all our simulations in order to match the observed abundance of galaxy clusters today, irrespective of the cosmology. We also used the same spectral index $n = -1$ throughout in order to focus our attention on possible differences due to the dark energy contribution alone. For these choices, the models EDE1 and EDE2 are almost degenerate, but their proximity serves as a useful test for how well differences in the results can be detected even for small variations in the EDE parameters. This gives a useful illustration on how well one can hope to be able to distinguish them in practice and provides realistic data for testing the discriminative power of specific statistics.

For our largest calculations we used 512^3 particles in boxes of volume $100^3\,h^{-3}{\rm Mpc}^3$, resulting in a mass resolution of $m_p = 5.17 \times 10^8\ h^{-1}M_\odot$ and a gravitational softening length of $\epsilon = 4.2\,h^{-1}{\rm kpc}$, kept fixed in comoving coordinates. All the simulations were started at redshift $z_{\rm init} = 49$, and evolved to the present. For the simulations, we adapted the cosmological code GADGET-3 (based on Springel et al. 2001; Springel 2005) and the initial condition code N-GENIC, in order to allow simulations with a time-variable equation of state. These simulations can be used to determine the mass function also in the high-mass tail with reasonably small cosmic variance error, while at the same time probing down to interestingly small mass scales.

In Figure 3, we plot the expansion function of the EDE models relative to the ΛCDM case. We note that the only modification required in the simulation code was to update the expression for calculating the Hubble expansion rate, which needs to include the quintessence component. This term enters in both the kinematics and the dynamics of the cosmological models.

According to the Friedmann equation within a flat universe we have

$$H(a) = H_0 \left[\frac{\Omega_{m,0}}{a^3} + \Omega_{\rm de,0}\, \exp\left(-3 \int \left[1 + w\,(a)\right] {\rm d} \ln a \right) \right]^{1/2} . \quad (5)$$

The density of dark energy changes with the scale factor as:

$$\Omega_{\rm de}(z) = \Omega_{\rm de,0} \exp\left(-3 \int d \ln a \left[1 + w\,(a)\right] \right), \quad (6)$$

instead of simply being equal to $\Omega_{\rm de,0}$, as in the usual scenario. For $w = -1$, the behaviour of a cosmological constant is recovered.

If we interpret the modified expansion rate as being due to $w(z)$, as defined in equation (2), we find:

$$H^2\,(z)\,/H_0^2 = \Omega_{\rm de,0}\,(1+z)^{3+3\bar{w}_h(z)} + \Omega_{m,0}\,(1+z)^3\,, \quad (7)$$

where

$$\bar{w}_h\,(z) = \frac{w_0}{1 + b \ln\,(1+z)}, \quad (8)$$

and b is given by the Eqn. (3).

We can see that effectively the EDE models predict the observed effect of an acceleration in the expansion rate, and this has consequences on the global geometry of the Universe. We note that the dark energy term in Eqn. (6) just parametrizes our ignorance concerning the physical mechanism leading to an increase in expansion rate. However, once the dependence of H on the scale factor is fixed, the mathematical problem of calculating structure growth is then unambiguously defined.

The evolution of $\Omega_{\rm de,a}$ affects not only the expansion rate of the background but also the formation of structures. The primary influence of dark energy on the growth of matter density perturbations is however indirect and arises through the sensitive dependence of structure growth on the expansion rate of the universe. In Figure 4, we show the linear growth factor D divided by the scale

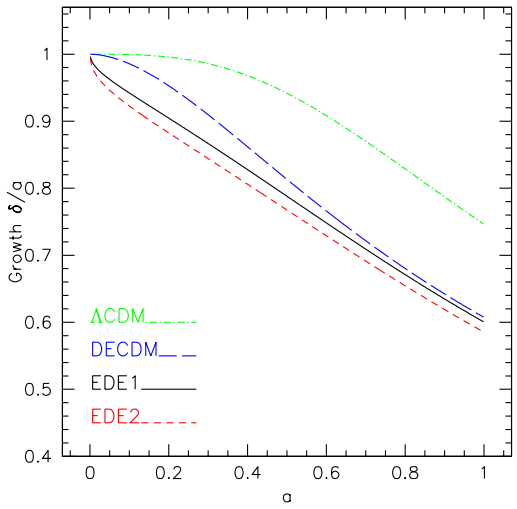

Figure 4. Ratio of the growth factor of linear density perturbations and the scale factor a, as a function of a. The four models are described in Table 1. The curves are normalized to unity at early times, i.e. we here assume that the starting density contrast is the same in the four cosmologies. The models EDE1 and EDE2 show a significant difference in the growth factor evolution even with small energy density at high redshift: structures have to grow earlier to reach the same abundance as the ΛCDM model today.

factor D/a as a function of time for all our models. All curves are normalized so that they start from unity at early times.

In order to rescale the power spectrum of matter fluctuations to the redshift of the initial conditions ($z = 49$ for all simulations), we introduced in our initial condition code the calculation of the growth factor for a general equation-of-state as given by Linder & Jenkins (2003):

$$D'' + \frac{3}{2}\left[1 - \frac{w(a)}{1+X(a)}\frac{D'}{a} + \frac{3}{2}\frac{X(a)}{1+X(a)}\frac{D}{a^2}\right] = 0, \qquad (9)$$

where $X(a)$ is the ratio of the matter density to the energy density:

$$X(a) = \frac{\Omega_{m,0}}{\Omega_{\rm de,0}} \exp\left[-3\int_a^1 d\ln a' w\left(a'\right)\right], \qquad (10)$$

and we allowed for a time-dependent equation of state, $w(a)$. Here we define the growth factor as the ratio $D = \delta(a)/\delta(a_i)$ of the perturbation amplitude at scale factor a relative to the one at a_i, and we use the normalization condition $D(a_{\rm eq}) = a_{\rm eq}$.

We can easily see that for very large redshift we recover the matter dominated behaviour in the ΛCDM case: $D(a) \propto a$. On the other hand, as expected, the linear growth in the two EDE models falls behind the green curve in Fig. 4, implying that they reach a given amplitude at earlier times. In fact, the expansion rate in the ΛCDM cosmology is lower than in EDE models, which governs the friction term $(\dot{a}/a)$ in the growth equation

$$\ddot{\delta} + 2\frac{\dot{a}}{a}\dot{\delta} - 4\pi G\rho\delta = 0 \qquad (11)$$

of the perturbations.

These formulae can be used to derive a suitable expression for the reduced linear overdensity δ_c for collapse expected in EDE models (Bartelmann et al. 2006), which in turn suggests that there are significant consequences for the process of non-linear structure formation, an expectation that we will analyse later in detail. In sum, structures need to grow earlier in EDE models than in ΛCDM in order to reach the same amplitude at the present time. At an equal redshift, the initial conditions must hence be more evolved in order to produce comparable results today. The DECDM shows a behaviour qualitatively similar to EDE1 and EDE2 (blue long-dashed line).

[H]

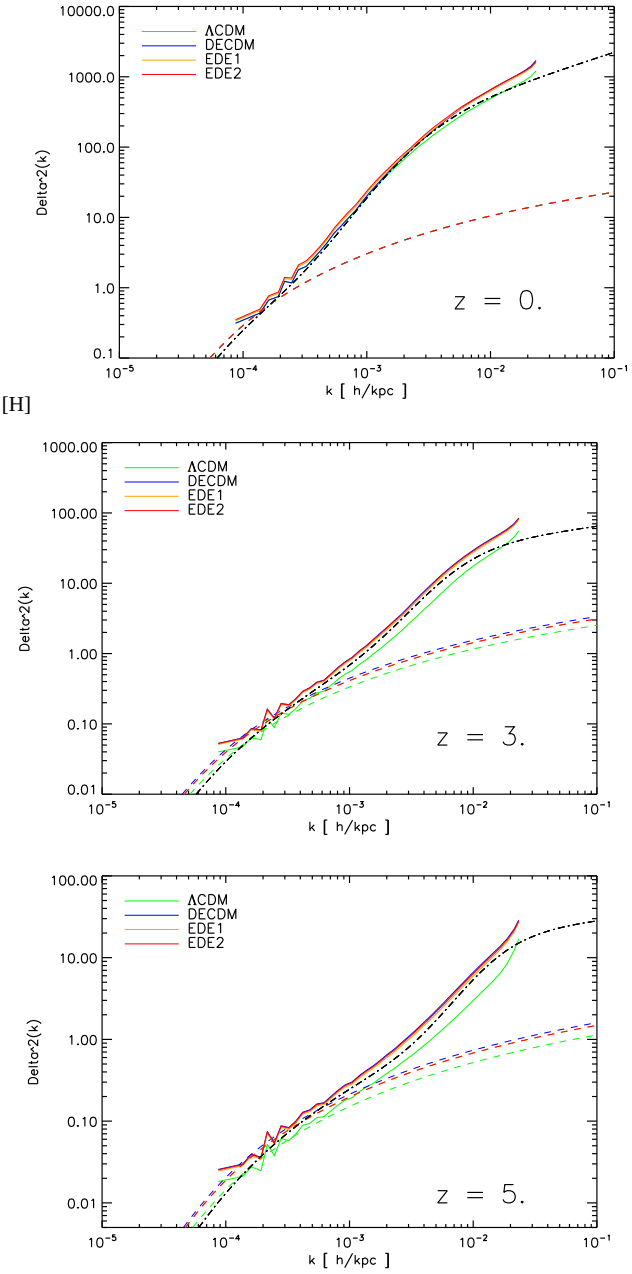

Figure 5. Comparison of the non-linear power spectra of the four different cosmological models studied here. The three panels give results for redshifts $z = 0$, $z = 3$ and $z = 5$, from top to bottom. The y-axes shows the dimensionless power $\Delta^2 = k^3 P(k)$ as a function of k computed from the dark matter density field using a grid of 512^3 points. All the simulations are normalized to $\sigma_8 = 0.8$ for the linearly extrapolated density field today. The dashed lines indicate the expected linear power spectra. The prediction from Smith et al. (2003) for the ΛCDM cosmology is shown by the black dot-dashed line.

In all our simulations, we have identified dark matter halos using two methods: the friends-of-friends (FOF) algorithm with linking length $b = 0.2$, and the spherical overdensity (SO) group finder. Candidate groups with a minimum of 32 particles were retained by the FOF group finder. In the SO algorithm, we first identify FOF groups, and then select the particle with the minimum gravitational potential as their centres, around which spheres are grown that enclose a fixed prescribed mean density $\Delta \times \rho_{\rm crit}$, where $\rho_{\rm crit}$ is the critical density. Different definitions of virial overdensity are in use in the literature, and we consider different values for Δ where appropriate. The classical definition of NFW adopts $\Delta = 200$ independent of cosmology, while sometimes also $\Delta = 200\,\Omega_m$ is used, corresponding to a fixed overdensity relative to the background density. Finally, a value of $\Delta \sim 178\,\Omega_m^{0.45}$ based on a generalization of the spherical top-hat collapse model to low density cosmologies can also be used. Note however that this may in principle depend on the dark energy cosmology (Bartelmann et al. 2006), and is hence slightly ambiguous in these cosmologies.

We have verified the correctness of our implementation of early dark energy in the simulation code by checking that it accurately reproduces the expected linear growth rate in these non-standard cosmologies. Recall that rather than normalizing the density perturbations of the initial conditions to the same value at the (high) starting redshift, we determine them such that they should grow to the same linear amplitude today in all of the models. In practice, we fix σ_8, the linearly extrapolated *rms* fluctuations in top-hat spheres of radius $8\,h^{-1}{\rm Mpc}$ to the value 0.8 for the epoch $z = 0$.

In Figure 5, we show measurements of the power spectrum of our different models at three different redshifts. While the models differ significantly at high redshift, the four different realizations show the same amplitude of the power spectrum, at least on large scales, at redshift $z = 0$ (left panel). The fluctuations on small scales probably reflect the earlier structure formation time in the EDE models and the resulting differences in the non-linear halo structures. The good agreement of the power spectrum at the end, as well as a detailed comparison of the growth rate of the largest modes in the box with the linear theory expectation (not shown), demonstrate explicitly that the EDE models are simulated accurately by the code, as intended.

Note also that the power spectrum measurements show that due to the slower evolution of the linear growth factor in EDE models, the degeneracy between the models is lifted towards high-z since this corresponds to more time for the different growth dynamics to take effect. Consequently, we expect a different evolution of structures back in time. Our main focus in the following will be to study the impact of a different equation of state for the dark energy upon the mass function of dark matter halos and its evolution with redshift.

4 THE MASS FUNCTION

In this section we measure the halo abundance at different redshifts and compare with analytic fitting functions proposed in the literature. Our primary goal is to see to which extent dark energy models can still be described by these fitting formulae, and whether there is any numerical evidence that supports the higher halo abundance predicted for the EDE cosmologies (Bartelmann et al. 2006). We will mostly focus on halo mass functions determined with the FOF algorithm with a linking length of 0.2, but we shall also consider SO mass functions later on.

In Figure 7, we show our measured halo mass functions in terms of the multiplicity function, which we define as

$$f\,(\sigma, z) = \frac{M}{\rho_0}\,\frac{{\rm d}n(M,z)}{{\rm d}\ln\sigma^{-1}} \qquad (12)$$

where ρ_0 is the background density, $n(M, z)$ is the abundance of halos with mass less than M at redshift z, and σ is the mass variance of the power spectrum filtered with a top-hat mass scale equal to M. We give results for the cosmological models ΛCDM, DECDM, EDE1 and EDE2, plotted as symbols, while the solid lines show various theoretical predictions.

Note that we plot the mass function only in a limited mass range in order to avoid being dominated by counting statistics or resolution effects. To this end we only consider halos above a minimum size of 200 particles. At the high mass end, individual objects are resolved well, but the finite volume of the box limits the number of massive rare halos we can detect. We therefore plot the mass function only up to the point where the Poisson error reaches $\sim 14\%$ (corresponding to minimum number of ~ 50 objects per bin).

As is well known, the Press & Schechter mass function (Press & Schechter 1974), while qualitatively correct, disagrees in detail with the results of N-body simulations (Efstathiou et al. 1988; White et al. 1993; Lacey & Cole 1994; Eke et al. 1996), specifically, the PS formula overestimates the abundance of halos near the characteristic mass $M_\star$ and underestimates the abundance in the high-mass tail. We therefore omit it in our comparison. The discrepancy is largely resolved by replacing the spherical collapse model of the standard Press & Schechter theory with the refined ellipsoidal collapse model (Sheth & Tormen 1999; Sheth et al. 2001; Sheth & Tormen 2002). Indeed, in the top left panel of Figure 6 we can see quite good agreement of the Sheth & Tormen mass function (ST) with our simulations at $z = 0$. We stress that here the standard value of $\delta_c = 1.689$ for the linear collapse threshold has been used irrespective of the cosmological model. Two other well-known fitting formulae are that from Jenkins (central panel, Jenkins et al. 2001, 'J') and that from Warren (right panel, Warren et al. 2006, 'W'), which differ only very slightly in the low-mass range. We compare our measurements with these models in the panels of the middle and right columns. As we can see from the comparison between the solid lines and the numerical data points, the differences between the different theoretical models (which only rely on the linearly evolved power spectrum at each epoch) and the simulation results is very small.

Figure 7 shows the redshift evolution of the mass function, in the form of separate comparison panels at redshifts $z = 1$ and $z = 3$. While at $z = 0$ the different cosmologies agree rather well with each other, as expected based on the identical linear power spectra, at redshift $z = 1$ we begin to see differences between the models, and finally at $z = 3$, we can observe a significantly higher number density of groups and clusters in the non-standard dark energy models. Notice that the model with constant w (blue line) behaves qualitatively rather similar to the EDE models. In each of the panels, we include a separate plot of the residuals with respect to the analytic fitting functions. This shows that at $z = 3$ the agreement is clearly best for the ST formula.

The differences between the models are most evident in the exponential tail of the mass function where it begins to fall off quite steeply, in agreement with what is expected from the power spectrum analysis. We can see that, at high-z, replacing the cosmological constant by an early dark energy scenario has a strong impact on the history of structure formation. In particular, non-linear struc-

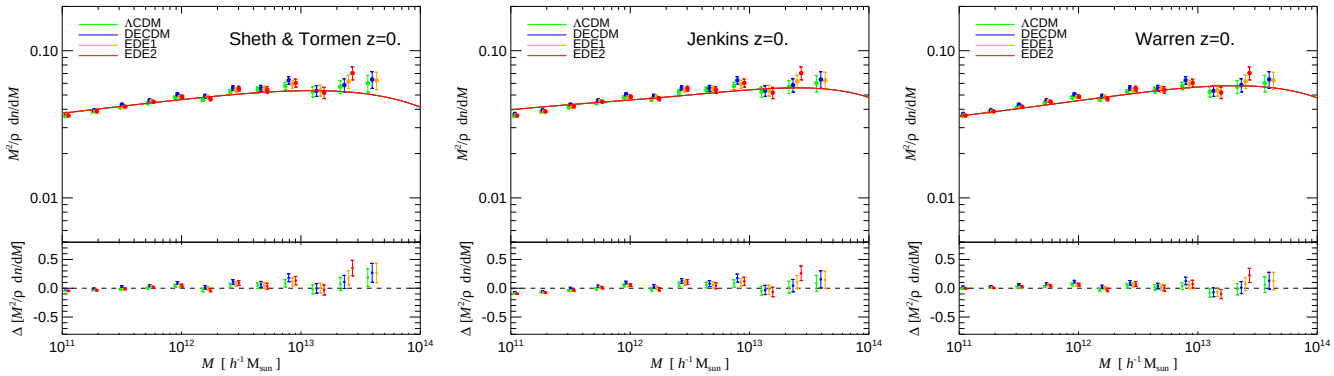

Figure 6. Friends-of-friends multiplicity mass functions at $z = 0$ for the four dark energy models studied here. The solid lines in each panel represent the multiplicity function computed analytically either from the Sheth & Tormen formula (left panel), the Jenkins formula (central panel) or the Warren model (right panel). The symbols are the numerical simulation results for ΛCDM (green), DECDM (blue), EDE1 (orange) and EDE2 (red). We consider only halos with more than 200 particles and we apply an upper mass cut-off where the Poisson error reaches 14%. In the lower plot of each figure we show the residuals between analytically expected and numerically determined mass functions for all models. The differences are typically below 10%. The error bars show Poisson uncertainties due to counting statistics for all models. At $z = 0$, the simulation results for all cosmologies are basically identical, which reflects the fact that we normalized the models such that they have the same linear power spectra today, with a normalization of $\sigma_8 = 0.8$.

tures form substantially earlier in such a model, such that a difference in abundance of a factor of ~ 2 is reached already by $z = 3$. This underlines the promise high redshift cluster surveys hold for distinguishing different cosmological models, and in particular for constraining the dynamical evolution of dark energy.

We now want to assess in a more quantitative fashion the differences between our numerical halo mass functions and the analytic fitting functions. In particular we are interested in the question whether we can objectively determine a preference for one of the analytic models, and whether there is any evidence that the ordinary mass function formalism does work worse for the generalized dark energy models than for ΛCDM. The latter would indicate that the critical linear overdensity threshold δ_c needs to be revised for EDE models, as suggested by the analytic spherical collapse theory (Bartelmann et al. 2006).

To this end we directly measure the goodness of the fit, which we define for the purposes of this analysis as:

$$\chi^2 = \left(\sum_j 1/\sigma_j^2 \right)^{-1} \sum_i \frac{(\mathrm{MF}_i - \mathrm{MF}_{\mathrm{TH},i})^2}{\sigma_i^2\, \mathrm{MF}_{\mathrm{TH},i}^2}, \qquad (13)$$

where $\mathrm{MF}_{\mathrm{TH},i}$ are the theoretical values, MF_i are the simulations results, and we took into account a simple Poisson error in the definition of the goodness of fit. In Figure 8, we plot this value expressed in percent for all simulations when compared with the theoretical formulae of ST (solid line), Jenkins (dotted line) and Warren (dashed line). We cannot identify a clearly superior behaviour of any the three fitting functions, at least at this level of resolution; the models lie in a strip between approximately 5 and 15% error between $z = 0$ and $z = 5$. There is some evidence that the ST model does a bit better than the other fitting formulae for the ΛCDM cosmology at high redshift, but the opposite is true for the two EDE cosmologies and the Jenkins and Warren functions.

Interestingly, the overall agreement between simulation results and fitting functions is actually slightly worse for ΛCDM than for the non-standard dark energy cosmologies. There is hence no tangible evidence that a revision of the mass function formalism is required to accurately describe EDE cosmologies. Our finding of a universal $f(\sigma)$ is quantitatively different from the expectation based on the analysis of the EDE models by Bartelmann et al. (2006). We find that only the different linear growth rate has to be taken into account for describing the mass function in the early dark energy cosmologies with the ST formalism, but there is no need to modify the linear critical overdensity value. To make this point more explicit, we show in Figure 10 the mass function for the EDE models and compare it to standard ST (solid lines), and to the expectations obtained taking into account a different density contrast for EDE models (dashed lines). The predictions in the second case are based on the analytic study of Bartelmann et al. (2006) and the critical overdensity is proportional to $(a)^{3\Omega_{\mathrm{de,sf}}/5}$ (see Eqn. 4).[1] Clearly, the proposed modification of δ_c actually worsens the agreement, both for the halos selected according the FOF algorithm (top panel) or defined with respect to the virial overdensity (bottom panel).

In the plots we discussed above, we always employed the FOF halo finder with standard linking length of $b = 0.2$ to find the halos, and the masses were simply the FOF group masses, which effectively correspond to the mass within an isodensity surface of constant overdensity relative to the background density. As the analytic mass function formulae have been calibrated with FOF halo mass functions, we expect that they work best if the mass is defined in this way. However, we may alternatively also employ a different mass definition based on the spherical overdensity (SO) approach, which allows one to take into account the time-dependent virial overdensity Δ predicted by generalizations of the spherical collapse model for dark energy cosmologies. In the bottom panel of Figure 10 we can see that an even more marked disagreement results when we take into account this arguably more consistent halo definition.

To stress this conclusion, in Figure 9, we show the residuals of our SO halo mass functions compared with the Sheth & Tormen prediction, as a function of redshift and for our different cosmological models, using the same procedure already applied to the FOF halo finder results. In this case, the halos were defined as virialized regions that are overdense by a variable density threshold equal to

[1] In order to obtain the new values for the critical overdensity it is necessary to compute the virial overdensity by solving the equation of the generalized spherical collapse model.

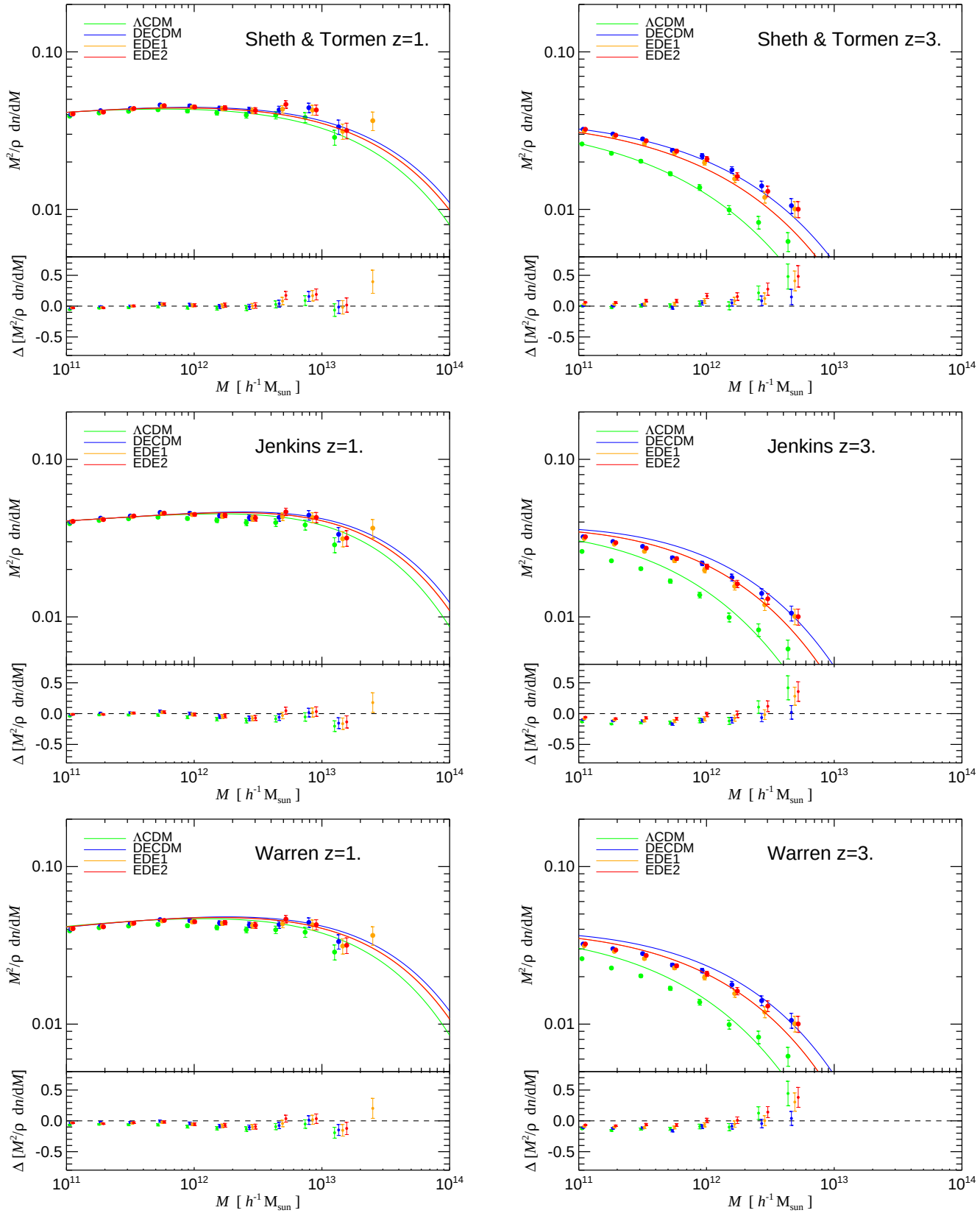

Figure 7. Friends-of-friends multiplicity mass functions for the four dark energy models studied here. The evolution towards high redshift is shown in terms of results at $z = 1$ (left column) and at $z = 3$ (right column). The solid lines in each plot represent the multiplicity function computed analytically from the Sheth & Tormen formula (top row), the Jenkins formula (middle row) and the Warren formula (bottom row). The points are the numerical simulation results for ΛCDM model (green), DECDM (blue), EDE1 (orange) and EDE2 (red). We consider only halos with more than 200 particles and we apply an upper mass cut-off where the Poisson error reaches 14%. In the lower plot of each figure we show the residuals between analytically expected and numerically determined mass functions for all models. The differences are typically below 15%. The error bars show Poisson uncertainties due to counting statistics for all models.

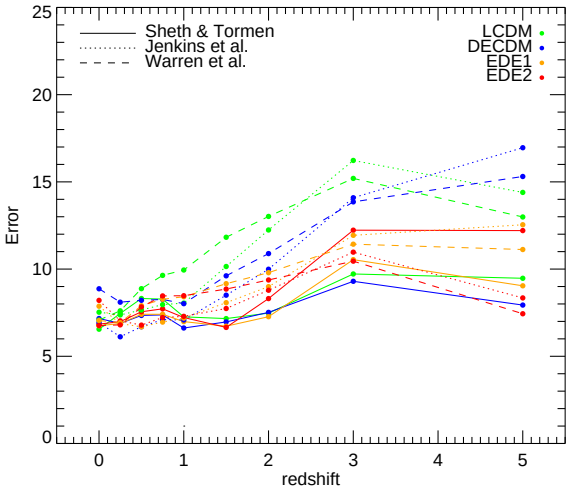

Figure 8. Redshift dependence of our goodness of fit parameter χ^2 (see Eqn. 13), expressed as percent, computed by comparing the theoretical expectation for the multiplicity mass function with the simulation results. All cosmological models are compared. The deviations are computed with respect to the Sheth & Tormen model (solid lines), the Jenkins et al. (dotted lines) and the Warren (dashed lines).

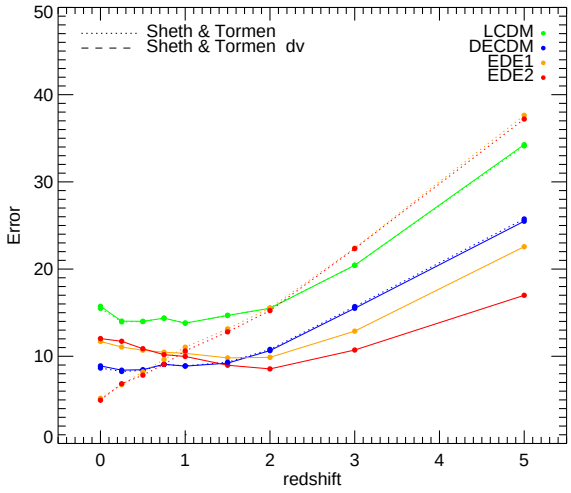

Figure 9. Redshift dependence of our goodness of fit parameter χ^2 (see Eqn. 13), expressed as percent, computed by comparing the theoretical expectation for the multiplicity mass function with the simulation results. All models are considered. Here we use the top hat halo mass definition to compute the mass function from the simulations, and the deviations are computed with respect to the standard Sheth & Tormen model (dotted-dashed lines), and the Sheth & Tormen formula computed from a generalization of the top-hat collapse theory (dashed lines).

$$\Delta_c = 18\pi^2 + 82x - 39x^2, \tag{14}$$

where $x = \Omega_m(z) - 1$, see Bryan & Norman (1998). This is the predicted dependence of Δ for ΛCDM, which we used for simplicity also for the other dark energy cosmologies. As expected, we see that the error increases relative to the FOF mass functions, with discrepancies of order 10% at $z = 0$. However, there is again no evidence that the non-standard dark energy cosmologies are described worse by the ST formalism than ΛCDM. Also, there is no improvement in the accuracy of the fit when we introduce the modified linear density contrast for the EDE models. On the contrary, as seen by the dotted lines, which represent the theoretical mass function (based on Sheth & Tormen) modified according to the spherical top hat collapse theory proposed by Bartelmann et al. (2006).

Our results thus suggest that the mass function depends primarily on the linear power spectrum and is only weakly, if at all, dependent on the details of the expansion history. This disagrees with the expectations from the generalization of the top hat collapse theory, which are not confirmed by our numerical data. In fact, our simulations show that a description of the mass function based on the generalized TH calculation is incorrect at the accuracy level reached here. While the dynamic range of our results could be improved by increasing the resolution and box-size of our simulations, it appears unlikely that this could affect our basic conclusions. Nevertheless, better resolution would be required if one seeks to still further reduce the present residuals of order 5-15% between the fitting functions of ST, Jenkins or Warren.

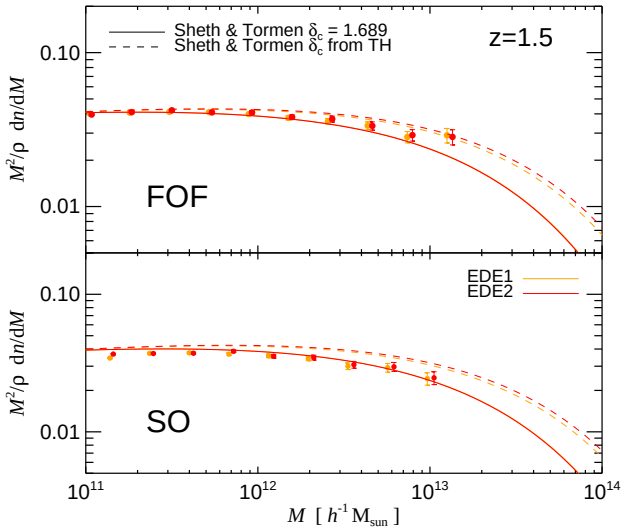

Figure 10. Multiplicity mass function at $z = 1.5$ for the two EDE models studied here. We want to highlight that the introduction of a modified overdensity motivated by the generalized spherical collapse theory (Bartelmann et al. 2006) reduces the agreement between the simulation results and the theoretical ST mass function. The measured points are in better agreement with the solid line (standard ST model) than with the dashed lines (ST modified model), the latter systematically overestimate the halo abundance. This holds true both if we consider the halos obtained from the FOF halo finder (top panel) or the one obtained by taking into account the theoretically motivated virial overdensity with the appropriate SO mass definition (bottom panel).

5 HALO PROPERTIES

5.1 The virial scaling relation

Evrard et al. (2008) have shown that the dark matter velocity dispersion of halos provides for accurate mass estimates once the relationship between mass and velocity dispersion is accurately calibrated with the help of numerical simulations. They have demon-

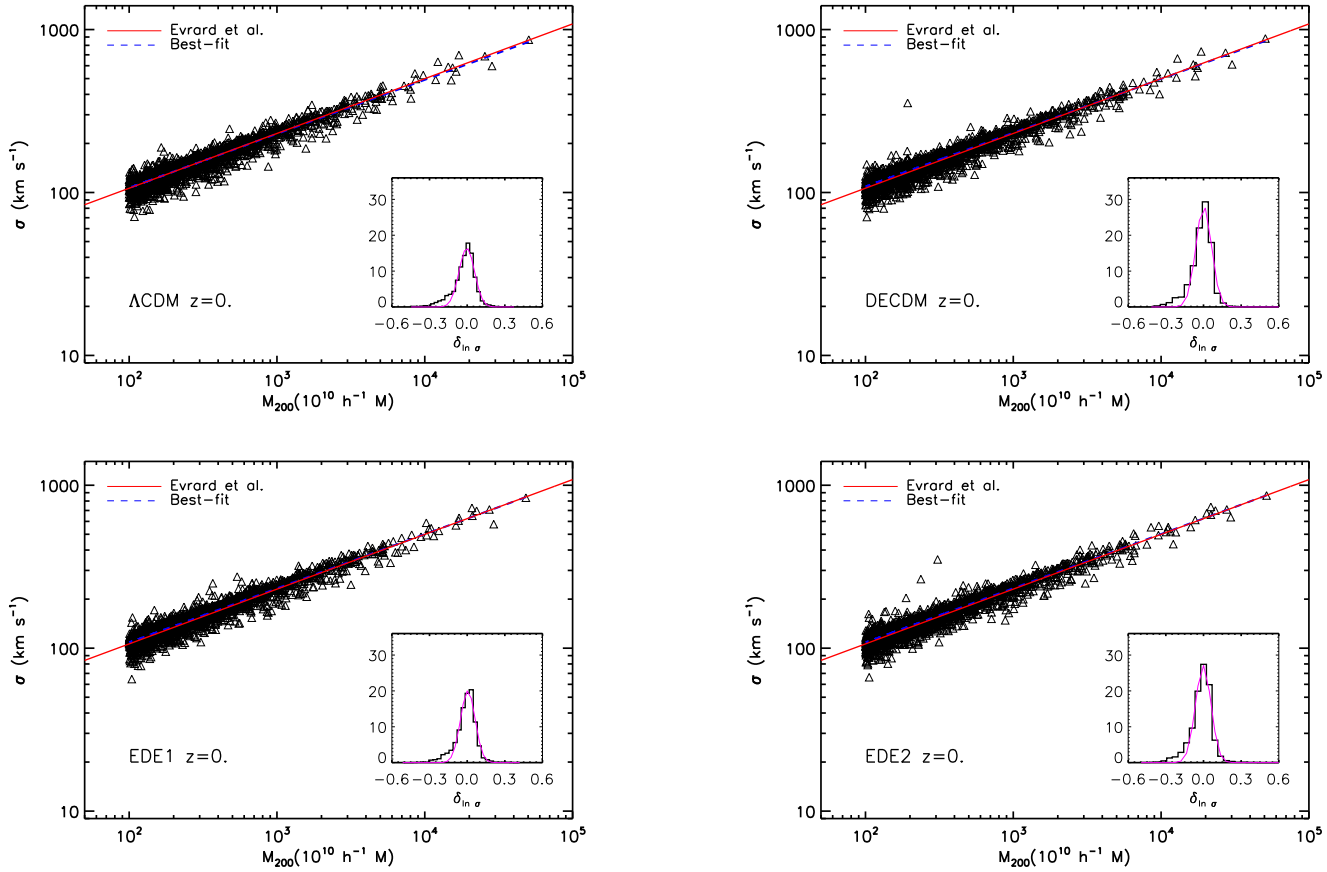

Figure 11. The virial scaling relation at the present epoch for primary halos with mass larger than $10^{12}\,\mathrm{M}_{\odot}$ for the four models considered (from left to right and top to bottom: ΛCDM, DECDM, EDE1, EDE2). The red solid line in each plot represents the Evrard et al. (2008) relation, while the blue dashed line is our best fit. The triangles are the simulation results: we employ a fixed critical threshold of $\Delta = 200$ to identify the dark matter halos. The insets show the distributions of deviations in $\ln \sigma_{\rm DM}$ around the Evrard et al. (2008) fit.

strated that there exists a quite tight power-law relation between the mass of a halo and its one-dimensional velocity dispersion $\sigma_{\rm DM}$, where

$$\sigma^2_{\rm DM} = \frac{1}{3N_p}\sum_{i=1}^{N_p}\sum_{j=1}^{3}|v_{i,j} - \bar{v_j}|^2\,, \qquad (15)$$

with $v_{i,j}$ being the $j_{\rm th}$ component of the physical velocity of particle i in the halo, N_p is total number of halo particles within a radius that encloses a mean overdensity of $\Delta = 200$ with respect to the critical density, and $\bar{v}$ is the mean halo velocity. When virial equilibrium is satisfied, we expect that the specific thermal energy in a halo of mass M and of radius R will scale with its potential energy, GM/R, while the kinetic energy is proportional to $M^{2/3}$. Since $\sigma_{\rm DM}$ expresses the specific thermal energy in dark matter, we can express the mean expected velocity dispersion as a function of mass as

$$\sigma_{\rm DM}\,(M,z) = \sigma_{\rm DM,15}\left(\frac{h(z)M_{200}}{10^{15}M_{\odot}}\right)^{\alpha}. \qquad (16)$$

Here the fit parameters are the slope α of the relation, and the normalization $\sigma_{\rm DM,15}$ at a mass scale of $10^{15}h^{-1}M_{\odot}$. While the slope α just follows from the virial theorem if halos form a roughly self-similar family of objects (which they do to good approximation), the amplitude $\sigma_{\rm DM,15}$ of the relationship is a non-trivial outcome of numerical simulations and reflects properties of the virialization process of the halos as well as their internal structure. Evrard et al. (2008) showed that a single fit is consistent with the numerical data of a large set of N-body simulations of the ΛCDM cosmology, covering a substantial dynamic range.

However it is conceivable that the amplitude of the relationship will be slightly different in early dark energy cosmologies, as a result of the different virial overdensity that is predicted by the top hat collapse in these cosmologies. If true, this would then also hint at a different normalization of the relationship between total Sunyaev-Zeldovich decrement and mass, which would hence directly affect observationally accessible probes of the cluster mass function at high redshift.

We here test whether we can find any difference in this relationship for our different dark energy cosmologies. In Figure 11, we plot the velocity dispersion of halos as a function of mass, in the four different cosmologies we simulated. The halos were identified using a spherical overdensity definition, where the virial radius r_{200} was determined as the radius that encloses a fixed multiple of 200 times the critical density at the redshift z, and M_{200} being the corresponding enclosed mass. We then determined the best-fit relation obtained from our numerical data (red solid lines). This fit is in very good agreement with the results obtained by Evrard et al. (2008) (dotted blue lines), given by $\sigma_{\rm DM,15} = 1082 \pm 4.0\,\mathrm{km\,s^{-1}}$ and $\alpha = 0.3361 \pm 0.0026$, a value consistent with the viral expectation of $\alpha = 1/3$. The insets show the residuals about the fit at redshift

$z = 0$. They have a log-normal distribution with a maximum of 6% dispersion (for the DECDM model) around the power-law relation. The histograms are well fit by a log-normal with zero mean.

We find that the halos closely follow a single virial relation, insensitive of the cosmological parameters, the epoch and also the resolution of the simulation. In particular, we do not find any significant differences for the EDE models, instead, the same form of the virial relation is preserved across the entire range of mass and redshift in the four simulations. The velocity dispersion-mass correlation hence appears to be global and very robust property of dark matter halos which is not affected by different contributions of dark energy to the total energy density of the universe.

This is a reassuring result as it means that also in the case of early dark energy, clusters can be studied as a one parameter family and the calibration of dynamical mass estimates from internal cluster dynamics does not need to be changed. Differences in the normalization should only reflect more or less frequent halo mergers and interactions, which can introduce an additional velocity component (Espino-Briones et al. 2007; Faltenbacher & Mathews 2007).

5.2 Halo concentrations

As we have seen, for an equal normalization of the present-day linear power spectrum, the dark matter halo mass function at $z = 0$ does not depend on the nature of dark energy. On one hand this is a welcome feature, as it simplifies using the evolution of the mass function to probe the expansion history of the universe, but on the other hand it disappointingly does not provide for an easy handle to tell different evolutions apart based only on the present-day data. However, a discrimination between the models may still be made if the *internal structure* of halos is affected by the formation history, which would show up for example in their concentration distribution.

Cosmological simulations have consistently shown that the spherically averaged mass density profile of equilibrium dark matter halos are approximately universal in shape. As a result, we can describe the halo profiles by the NFW formula (Navarro et al. 1995, 1996, 1997):

$$\frac{\rho\,(r)}{\rho_{\rm crit}} = \frac{\delta_c}{(r/r_s)(1+r/r_s)^2}, \tag{17}$$

where $\rho_{\rm crit} = 3H_0^2/8\pi G$ is the critical density, δ_c is the characteristic density contrast and r_s is the scale radius of the halo. The concentration c is defined as the ratio between r_{200} and r_s. The quantities δ_c and c are directly related by

$$\delta_c = \frac{200}{3}\frac{c^3}{[\ln(1+c) - c/(1+c)]}. \tag{18}$$

The concentration c is the only free parameter in Eqn. (18) at a given halo mass and these two quantities are known to be correlated. In fact, characteristic halo densities reflect the density of the universe at the time the halos formed; the later a halo is assembled, the lower is its average concentration.

We have measured concentrations for our halos in the different cosmologies using the same procedures as applied to the analysis of the Millennium simulation (Neto et al. 2007; Gao et al. 2008). For our measurements, we take into account both relaxed and unrelaxed halos. In the second case, the equilibrium state is assessed by means of three criteria: (1) the fraction of mass in substructures with centers inside the virial radius is small, $f_{\rm sub} < 0.1$, (2) the normalized offset between the center-of-mass of the halo $\boldsymbol{r}_{\rm cm}$ and the potential minimum $\boldsymbol{r}_c$ is small, $s = |\boldsymbol{r}_c - \boldsymbol{r}_{\rm cm}|/r_{200} < 0.07$ and (3) the virial ratio is sufficiently close to unity, $2\,T/|U| < 1.35$. These quantities provide a measure for the dynamical state of a halo, and considering these three conditions together guarantees in practice that a halo is close to an equilibrium configuration, excluding the ones with ongoing mergers, or with strong asymmetric configurations due to massive substructures.

For all relaxed halos selected in this way, we computed a spherically averaged density profile by storing the halo mass in equally spaced bins in $\log_{10}(r)$ between the virial radius r_{200} and $\log_{10}(r/r_{200}) = -2.5$. We used 32 bins for each halo and we choose a uniform radial range in units of r_{200} for the fitting procedure so that all halos are treated equally, regardless of the mass. We find that we obtain stable results when we use halos with more than 3000 particles, consistent with the Power et al. (2003) criteria, while with fewer particles we notice resolution effects in the concentration measurements, as both the gravitational softening and discreteness effects can artificially reduce the concentration. The final mass range we explored is hence 10^{12} to $10^{15}\,h^{-1}{\rm M}_\odot$.

In Figure 12, we show our measured mass-concentration relation for the different dark energy models at $z = 0$. The four solid lines show the mean concentration as a function of mass. The boxes represent the 25 and 75 percentiles of the distribution, while the whiskers indicate the 5 and 95 percentiles of the distributions. We note that the scatter of the concentration at a given mass is very close to a log-normal distribution. It is interesting to remark that both the mean and the dispersion decrease with mass. In fact, massive halos form in some sense a more homogeneous population, because they have collapsed recently and so the formation redshift is relatively close to the present epoch. On the other hand, less massive halos have a wider distribution of assembly redshifts and the structure of individual objects strongly depends on their particular accretion histories. For them, the assumption that objects we observe are just virialized is therefore inappropriate, especially for very low mass halos. In Fig. 12 we take into account only the relaxed halos, but we did an analogue measurement also for the whole sample, shown in Figure 13 at redshift 0 (top panel) and at $z = 1$ (low panel).

The correlation between mass and concentration approximately follows a power law for the relaxed halos of the ΛCDM model. In the literature, the concentrations would be expected to be somewhat lower if a complete sample is considered that includes disturbed halos. Comparing Figures 12 and 13 we notice that this expectation is confirmed, but the difference is not very pronounced, only about 5% for the whole mass range. We also note that the normalization $\sigma_8 = 0.8$ used for our simulations slightly lowers the amplitude of the zero point of the relation (Macciò et al. 2008) when compared to the WMAP-3 normalization, as halos tend to assemble later with lower σ_8 and/or Ω_m.

When we compare our four simulated cosmologies we find that, as expected, EDE halos of given mass have always higher concentration at a given redshift than models with a cosmological constant: they tend to form earlier and so they have a higher characteristic density. Nevertheless, the differences are not large, they deviate by no more than $\sim 27\%$ at $z = 0$ over the entire mass range we studied for all halos and $\sim 25\%$ for the relaxed one. At higher redshift, the differences are only slightly bigger, of order of $\sim 28\%$ at $z = 1$ for the whole sample, and $\sim 35\%$ for halos in equilibrium configuration, suggesting that we anyway need reliable numerical calibrations and highly accurate observational data to discriminate between the different cosmologies. Interestingly, the average con-

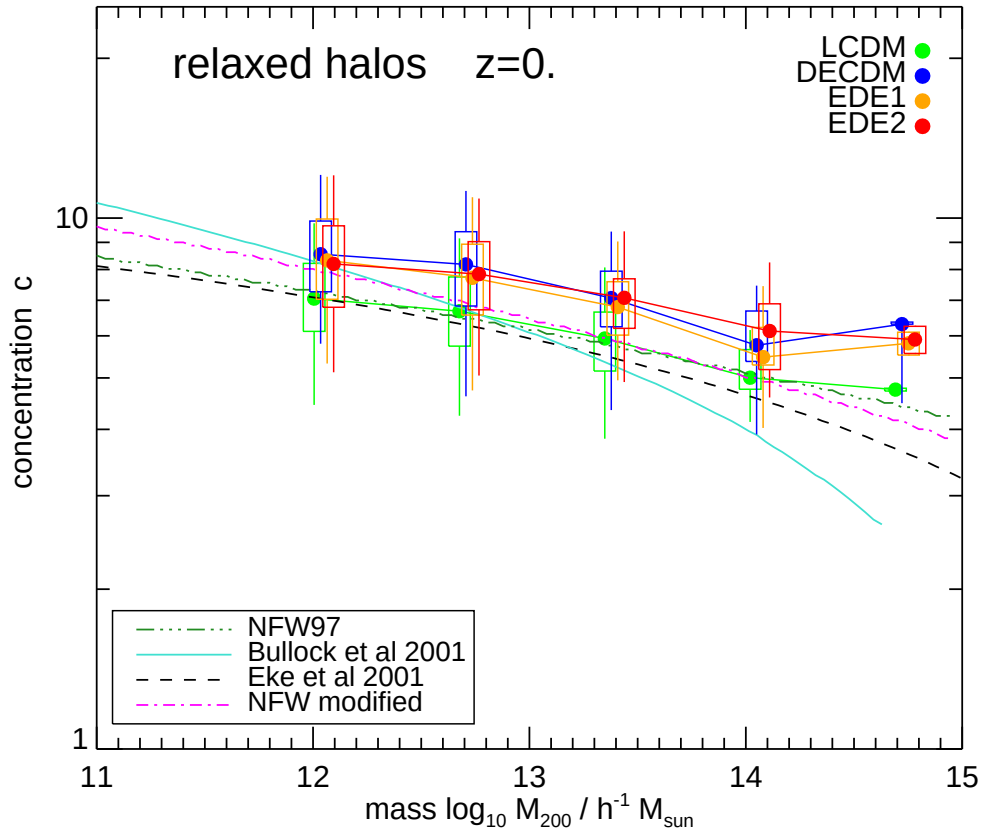

Figure 12. Mass-concentration relation for relaxed halos in all our simulations. The boxes represent the 25 and 75 percentiles of the distribution with respect to the median value, while the whiskers show the 5 and 95 percentiles. We compare our results with the theoretical expectations from NFW, ENS, B01. Also, a modified NFW prescriptions with slightly modified parameters as updated by Gao et al. (2008) is shown (see Section 5 for details).

centration is almost independent of mass when we consider $z \geqslant 2$, as the average concentration of the more massive halos is similar at all redshifts (Gao et al. 2008) and we are then restricted to the exponential tail of the mass function.

The change in concentration normalization relative to the cosmological constant model is well represented by the ratio between the linear growth factor of different models at very high redshift,

$$c_0 \rightarrow c_{0,\Lambda\mathrm{CDM}} \frac{D_+(\infty)}{D_{+,\Lambda\mathrm{CDM}}(\infty)}, \qquad (19)$$

as suggested by Dolag et al. (2004). In Table 2, we compare the ratio between the concentration at $z = 0$ both for the relaxed halos (second column) and for the whole sample (third column) with the ratio between the asymptotic growth factor for the same cosmologies (forth column). The order of magnitude of the two effects is comparable, although the match is not perfect. Here the ratios are computed for $M \sim 4 \times 10^{12}\ h^{-1} M_\odot$, where we have a large number density of halos.

It is interesting to compare the concentrations we measure with the various theoretical predictions that have been made for this quantity. We investigate three popular descriptions for the concentration: the classic Navarro, Frenk & White model (hereafter NFW), the model of Bullock et al. (2001, hereafter B01), and that of Eke et al. (2001, hereafter ENS). Finally, we also plot the new modified version of the original Navarro Frenk and White model, as recently proposed by Gao et al. (2008). Both the B01 model and

Model	$\frac{c_0}{c_{0,\Lambda\mathrm{CDM}}}$	$\frac{c_{0,ALL}}{c_{0,ALL,\Lambda\mathrm{CDM}}}$	$\frac{D_+(\mathrm{inf})}{D_{+,\Lambda\mathrm{CDM}}(\mathrm{inf})}$
ΛCDM	1.000	1.000	1.000
DECDM	1.256	1.275	1.228
EDE1	1.218	1.232	1.229
EDE2	1.255	1.273	1.252

Table 2. Concentration and asymptotic growth factor in the four different cosmologies studied here. The ratio between the concentration parameters at redshift $z = 0$ refers to a mass of $M \sim 4 \times 10^{12}\ h^{-1} M_\odot$ that corresponds to the mass range that contains the majority of our halos. For each model (first column) we give the c_0 parameter relative to ΛCDM, taking into account the relaxed halos (second column) or the whole sample (third column). Finally, in the last column we show the linear growth factor at infinity relative to the ΛCDM cosmology.

the standard NFW have two free parameters that have been tuned to reproduce simulation results. In the original NFW prescription, the definition of the formation time of a halo is taken to be the redshift at which half of its mass is first contained in a single progenitor: $F = 0.5$. The second parameter is the proportionality constant, $C = 3000$, that relates the halo density scale to the mean cosmic density at the collapse redshift z_{coll}. Recently, Gao et al. (2008) noticed that the evolution of the mass-concentration relation with redshift can be approximated much better by setting $F = 0.1$. The

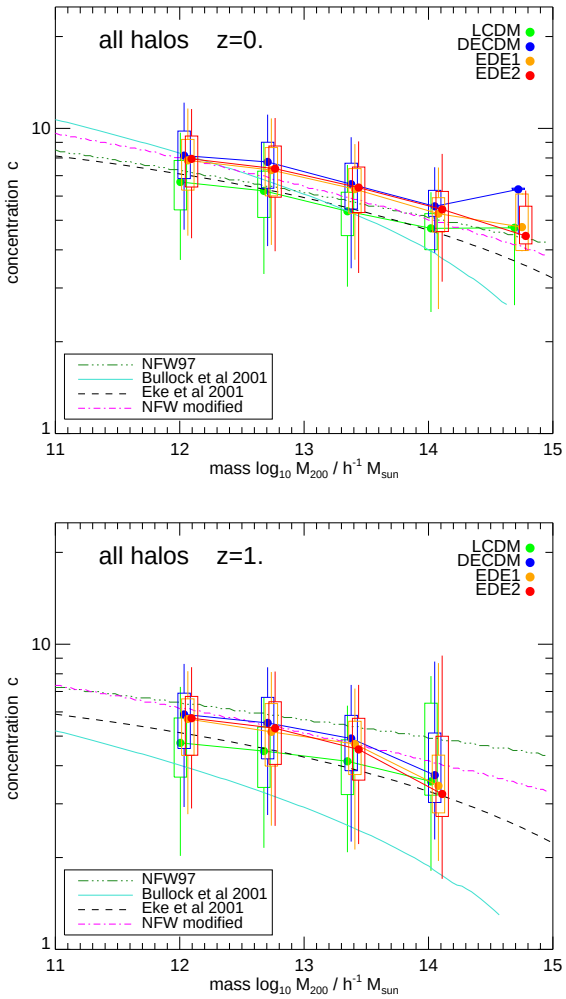

Figure 13. Mass-concentration relation for all halos in our simulations. The top panels refers to redshift $z = 0$, while the bottom panel shows the results at $z = 1$. The boxes represent the 25 and 75 percentiles of the distribution with respect to the median value, while the whiskers show the 5 and 95 percentiles. We compare our results with the theoretical expectations from NFW, ENS, B01. Also, a modified NFW prescription with slightly modified parameters as updated by Gao et al. (2008) is shown (see Section 5 for details). The concentration is 5% lower with respect to the relaxed sample at $z = 0$ for the ΛCDM model.

B01 model adopts as collapse redshift the epoch at which the typical collapsing mass fulfills $M_*(a_c) = F\,M_{\rm vir}$, with $F = 0.01$. They further assume that the concentration is a factor $K = 3.4$ times the ratio between the scale factor at the time the halo is identified and the collapse time. For K and F we use the values that are indicated as the best parameters by Macciò et al. (2007). Finally, we compute the ENS prescriptions considering the effective amplitude of the power spectrum at the scale of the cluster mass. This quantity, rescaled for the linear growth factor of the simulated cosmology, has to be constant. In this case, only one parameter, $C_\sigma = 28$, is needed. Bullock et al. (2001) and Eke et al. (2001) refer to the virial radius as the one including an overdensity given by the generalized top hat collapse model. We have appropriately adapted these models such that the concentration of a halo is defined instead relative to radius r_{200}, as in the NFW model.

Aside from B01, all three other model predictions yield concentrations that agree reasonably well with the measured values at $z = 0$. The B01 model underpredicts the relation at high masses, where it gives has a sharp decline of the relation for $M\ 10^{13}\ h^{-1}{\rm M}_\odot$ which is not seen in the simulations. In contrast, the NFW model is in reasonable agreement with the data at $z = 0$ for both halo samples. However, at $z = 1$ the evolution predicted by the NFW model is less than what we find numerically, even when we consider the revised formulation proposed by Gao et al. (2008) (indicated as NFW modified). The NFW model with the new fitting parameters yields a reasonable fit at the high mass end, but performs a bit worse than the original formulation at $z = 0$, specially at low masses. Unfortunately, for the NFW model the normalization is model dependent, so we cannot really capture all the effects due to different cosmological parameters we use. Finally, the dashed black line in each plot shows the ENS model. This prescription gives the best match with our results and has been able to reproduce the slope of the concentration-mass relation even at higher redshift.

At a fixed mass, halos in the EDE cosmology are significantly less concentrated than their counterparts in the ΛCDM cosmology. It is interesting to notice that the ENS model reproduces these differences quite well, without modifications of the original prescription. In Figure 14, we plot for each simulation the corresponding theoretical expectation (dashed lines) for the sample of relaxed halos at $z = 0$. For a low density universe the scaling of the linear growth factor with redshift leads to a greater difference between the models. Dark halo concentrations depend both on the redshift evolution of δ_c and the amplitude of the power spectrum on mass scales characteristic for the halo.

These results for the concentration are particularly important since they demonstrate that quintessence cosmologies with the same equation-of-state at present, but different redshift evolution, can produce measurable differences in the properties of the non-linear central regions of cluster-sized halos. However, the prospects to observationally exploit these concentration differences to distinguish different dark energy cosmologies are sobering. For one, the systematic differences we measure for the concentrations are quite small compared to the statistical errors for the mean concentration, while at the same time the theoretical algorithms for predicting the halo concentration perform quite differently already for the ΛCDM cosmology. Furthermore, directly measuring halo concentrations in observations is not readily possible as it requires an accurate knowledge of the virial radius of a halo, a parameter which is poorly constrained from observations. It therefore remains to be seen whether the effects of dark energy on the non-linear structure of dark halos can be turned into a powerful tool to learn about the nature of dark energy.

6 COUNTING HALOS BY VELOCITY DISPERSION

As we have seen, the different evolution of the halo mass function is in principle a very sensitive probe of the expansion history of the universe, especially when the massive end of the mass function is probed. Obtaining absolute mass estimates from observations is however problematic, and fraught with systematic biases and uncertainties. It is therefore important to look for new ways to count halos which are more readily accessible by observations.

One such approach lies in using the motion of galaxies in groups or clusters of galaxies to measure the line-of sight velocity dispersion, which in turn can be cast into an estimate of the total virial mass of the host halo. This relies on the assumption that the

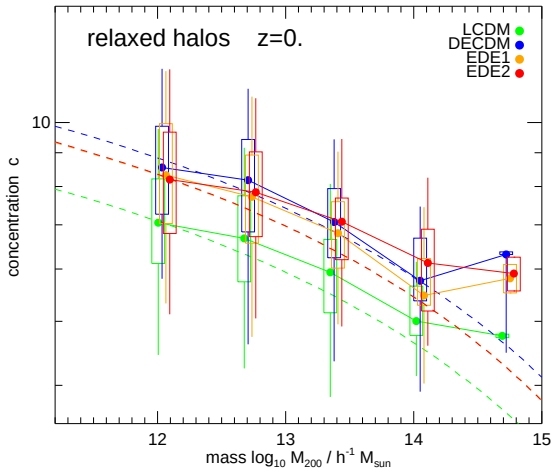

Figure 14. Mass-concentration relation for relaxed halos today. Here we show the agreement between simulation results (symbols) and theoretical predictions from ENS (dashed lines), both for the ΛCDM and EDE cosmologies. To this end we solve Eqn. (13) and (16) of Eke et al. (2001). The differences between the four cosmologies are due mostly to the differences in the growth factor evolution and consequently in the amplitude of the power spectrum. The ENS formula works quite well also for EDE models without modifications of the original prescription.

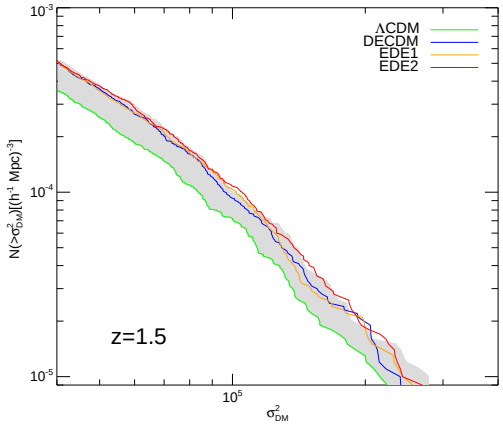

Figure 15. The velocity function $n(\sigma)$ as a function of halo mass, for all satellites inside r_{200}. The shaded area indicates the differences between a ΛCDM model with $\sigma_8 = 0.8$ and the same model with $\sigma_8 = 0.9$. It is interesting to remark that this EDE models could justify a higher normalization cosmology.

dynamics of the cluster or group galaxies is tracing out the dark matter halo potential.

Cluster and group galaxies can be identified with dark matter sub-structures in N-body simulations (Springel et al. 2001; Vale & Ostriker 2004). Employing the bulk velocities of sub-halos as a simulation proxy for real galaxy velocities, we can hence build a velocity profile for any isolated halo, and estimate a line-of-sight velocity dispersion, similarly as it is done for observed group catalogues of galaxies. This allows then to directly count halos (i.e. galaxy groups) as a function of line-of-sight velocity dispersion, bypassing the problematic point of assigning halo mass estimates.

In Figure 15, we show our estimated cumulative velocity dispersion function for our four different cosmologies at redshift $z = 1.5$. This graph can be interpreted as being a different representation of the halo mass function, except that it is in principle directly accessible by observations. For this measurement, we have derived the information on the velocities from the SUBFIND algorithm directly implemented in GADGET-3, which can find subhalos embedded in dark matter halos.

An important aspect of this statistic is that it does not rely on the often ambiguous definition of a group mass. Instead, it can be directly measured and is more readily accessed by observations. In fact, studies based on the DEEP2 survey (Lin et al. 2004; Davis et al. 2005; Conroy et al. 2007) indicate that, if combined with both the velocity dispersion distribution of clusters from the Sloan Digital Sky Survey and independent measurements of σ_8, they will be able to constrain w to within approximately 1% accuracy. This method is almost independent of cosmological parameters, with the exception of σ_8, since a change in normalization can shift the space density of halos as a function of mass by a similar amount as done by the EDE models. This is illustrated in Figure 15 by the shaded area, which represents the change of the velocity dispersion function when σ_8 is increased from 0.8 (green line) to 0.9 (upper limit of the shaded area). The velocity distribution function of the EDE models then approaches the one that we would measure for a ΛCDM model with higher σ_8.

These kind of studies have strong motivations both from the observational and theoretical point of view: there is little scatter between host galaxy luminosity and dark matter halo virial mass and the velocity difference distribution of satellites and interlopers can be modeled as a Gaussian and a constant, respectively (Conroy et al. 2005; Faltenbacher & Diemand 2006).

Figure 16 (left panel) shows the cumulative number of groups with velocity dispersion above a given value, as a function in redshift for the different models. We decided to count halos above a velocity dispersion of $300\,\mathrm{km\,s^{-1}}$, where accurate measurements can be expected also from observations. Note that there is already a very large difference between ΛCDM and EDE at redshift $z = 1$. We find that there is almost no evolution in the cluster number in the dark energy models, while ΛCDM drops by a factor of nearly 10 up to redshift $z = 3$. What is especially important here is the relative difference between the number counts of the two different cosmologies. The fact that we do not need to introduce the mass in this comparison give us the advantage of having no error derived from the particular measurement procedure adopted for the mass. At a fixed velocity dispersion, we can directly probe the growth of the structure at each redshift, which depends on the equation of state parameter w. The slower evolution of the cluster population in EDE models is exactly what is expected to be observed also from Sunyaev-Zeldovich studies of large samples of clusters of galaxies. Combined with probes of the cluster internal velocity dispersion we can hence hope to be able to derive stringent cosmological constraints.

We also remark that the relative difference between the number of objects within these four simulations seems to be a quite robust statistic which is invariant with respect to details of the measurement procedure. For example, in Figure 16 (right panel), we change the number of considered subhalos in the halos to be a minimum of 3, 4, and 5, but the velocity dispersion function relative to the ΛCDM cosmology is essentially unchanged. In practice, the number of observable satellites per host halo suffers from limitations imposed by the magnitude limit of the survey. Our results suggest that the measured velocity dispersion should however be relatively insensitive to this selection effect.

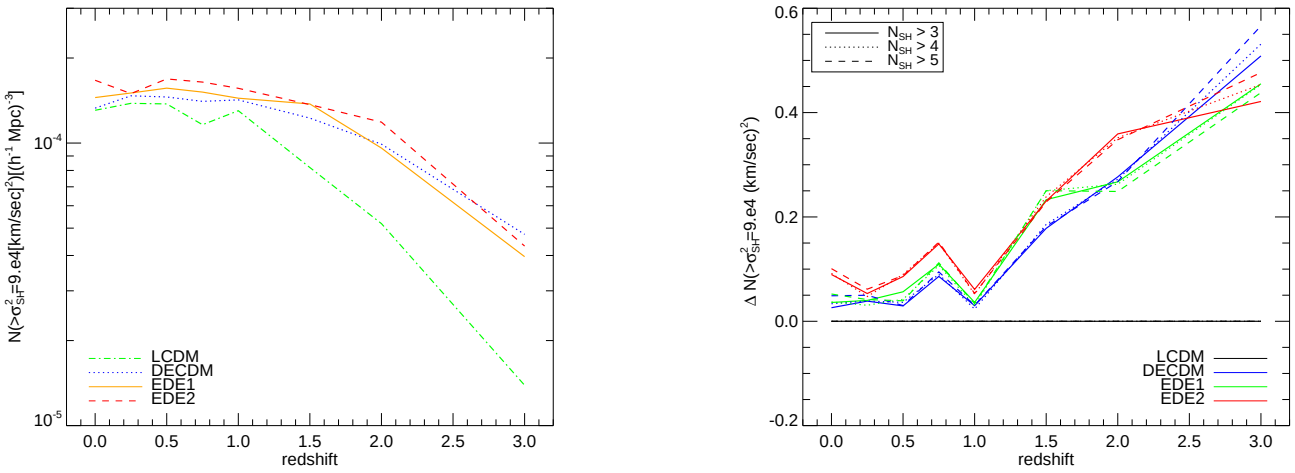

Figure 16. Left panel: Comparison of the redshift evolution of the velocity dispersion function for all four cosmologies we simulated (ΛCDM, DECDM, EDE1, and EDE2). Here the cumulative count of groups with velocity dispersion above $\sigma = 300\,\mathrm{km\,s^{-1}}$ was used to measure the amplitude of the velocity dispersion function. Right panel: Differences in the number count when only halos with more than 3 (solid line), 4 (dotted line) or 5 (dashed line) substructures are selected.

Finally, we have also studied a few properties of the largest substructures in halos to see whether there is a difference in EDE cosmologies. In Figure 17, the small diamonds indicate the values of the ratio between M_1 (the mass of the most massive subhalo) and M_{200} (the mass within a sphere of density 200 times the critical value at redshift 0) for the first 200 most massive halos at redshift $z = 3$. The filled circles represent the median of the distribution, computed in bins of 50 halos each, while the error bars mark the 20-th and 80-th percentiles of the distribution. There is almost no dependence on parent halo mass, but we can notice a small, but systematic tendency for the ΛCDM subhalos to be slightly more massive. The dependence is quite weak, yet this behaviour is clear even if the mass of the progenitor M_{200} tends to be lower on average at this high redshift. This is symptomatic of the fact that the ΛCDM substructures are formed at lower redshift with respect to what happens in the EDE models. This is also consistent with expectations based on the observed dependence of substructure mass fraction on halo mass (e.g. De Lucia et al. 2004). Once accreted onto a massive halo, subhalos suffer significant stripping, an effect that is more important for substructures accreted at higher redshift, making the subhalos in the EDE models less massive on average.

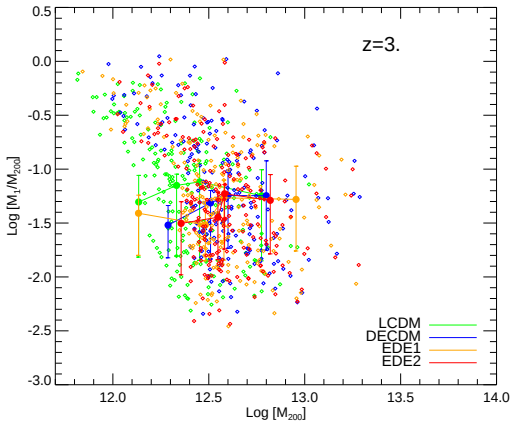

Figure 17. Ratio of the mass of the two most massive substructures with respect to the mass of the parent halo. The small diamonds refer to individual halos, while the filled circles are the median values. The error bars mark the 20th and 80th percentiles of the distributions.

7 CONCLUSIONS

In this study we have analyzed non-linear structure formation in a particular class of dark energy cosmologies, so called *early dark energy* models where the contribution of dark energy to the total energy density of the universe does not vanish even at high redshift, unlike in models with a cosmological constant and many other simple quintessence scenarios. Our particular interest has been to test whether analytic predictions for the halo mass function still reliably work in such cosmologies. As the evolution of the mass function is one of the most sensitive probes available for dark energy, this is of crucial importance for the interpretation of future large galaxy cluster surveys at high redshift. The mass function of EDE models is also especially interesting because analytic theory based on extensions of the spherical collapse model predicts that the mass function should be significantly modified (Bartelmann et al. 2006), and in particular be characterized by a different value of the linear overdensity δ_c for collapse, as well as a slightly modified virial overdensity.

We have carried out a set of high-resolution N-body simulations of two EDE models, and compared them with a standard ΛCDM cosmology, and a model with a constant equation of state equal to $w = -0.6$. Interestingly, we find that the universality of the standard Sheth & Tormen formalism for estimating the halo mass function also extends to the EDE models, at least at the $\lesssim 15\%$ accuracy level that is reached also for the ordinary ΛCDM model. This means that we have found good agreement of the standard ST estimate of the abundance of DM halos with our numerical results for the EDE cosmologies, *without* modification of the assumed virial overdensity and the linear density contrast threshold. This disagrees with the theoretical suggestions based on the generalized top-hat collapse. In fact, if we instead use the latter as theoretical prediction of the halo mass function, the deviations be-

tween the prediction and the numerical results become significantly larger. We hence conclude that the constant standard value for the linearly extrapolated density contrast can be used also for an analysis of early dark energy cosmologies. Very recently, similar results were also obtained by Francis et al. (2008), who studied the same problem in cosmological simulations with somewhat smaller mass resolution.

This results on the mass function appear to hold over the whole redshift range we studied, from $z = 0$ to $z = 3$. Since our simulations were normalized to the same σ_8 today, their mass functions and power spectra agree very well today, but towards higher redshift there are significant differences, as expected due to the different histories of the linear growth factor in the different cosmologies. In general, structure in the EDE cosmologies has to form significantly earlier than in ΛCDM to arrive at the same abundance today. For example, already by redshift $z = 3$, the abundance of galaxy clusters of mass $M = 5 \times 10^{12}\, h^{-1}\mathrm{M}_\odot$ is higher in EDE1 by a factor of ~ 1.7 relative to ΛCDM.

The earlier formation of halos in EDE models is also directly reflected in the concentration of halos. While for a given σ_8 we find the same abundance of DM halos, the different formation histories are still reflected in a subtle modification of the internal structure of halos, making EDE concentrations for all halo masses and redshifts considered slightly higher. The difference is however quite small, but it would, for example, lead to a higher rate of dark matter annihilation in halos.

Another relationship that appears to accurately hold equally well in ΛCDM as in generalized dark energy cosmologies is the virial scaling between mass and dark matter velocity dispersion that Evrard et al. (2008) has found. In fact, we find that their normalization of this relation is accurately reproduced by all of our simulations within the measurement uncertainties, independent of cosmology. This also suggests that possible differences in the virial overdensity of EDE halos must be very small, and that presumably the relationship between total Sunyaev-Zeldovich decrement and halo mass is unmodified as well.

We show that counting the number of halos as a function of the line-of-sight velocity dispersion (of subhalos or galaxies), both in simulations and observations, can probe the growth of structures with redshift, and so put powerful constraints on the equation of state parameters. This goal can be achieved by just identifying and counting groups in galaxy survey data such as DEEP2, and by comparing them with high-resolution N-body simulations. Precision measurements with this technique will still require accurate calibrations to deal with complications such as a possible velocity bias or selection effects in observational surveys. However, Davis et al. (2005) suggest that the DEEP2 survey alone has the power to constrain w to an accuracy of 20% using velocity dispersion data, which illustrates the promise of this technique. In combination with other independent data, such as X-ray temperature and SZ decrement data, the constraints could be improved to an accuracy of 5%, without the need to invoke a model for the ambiguous total mass of a halo.

Distinguishing a time-varying dark energy component from the cosmological constant is a major quest of the present theoretical and observational astronomy. One approach is to rely on classical cosmological tests of the Hubble diagram, e.g. by pushing the supernova type Ia observations to much higher redshift. Another quite direct geometrical probe is the observation of baryonic acoustic oscillations in the matter distribution at different redshifts. Finally, the linear and non-linear evolution of cosmic structures provides another opportunity to constrain dark energy. In this work we have used numerical N-body simulations to examine the difference in structure growth in early dark energy cosmologies. We have seen that such simulations are essential to test the predictions of more simplified analytic models, and to calibrate observational tests that try to constrain the properties of dark energy with the abundance and internal structure of dark matter halos. Our results show clearly that the effects due to dynamical dark energy tend to be quite subtle, and can only be cleanly distinguished from ordinary ΛCDM in high accuracy simulations. This poses new challenges to improve the precision of future generations of simulations, and at the same time emphasizes the immense observational task to arrive at sufficiently precise data at high redshift to constrain the dark side of the universe with the required accuracy.

ACKNOWLEDGEMENTS

We acknowledge Matthias Bartelmann for providing us with his code LIBASTRO for the virial overdensity prediction in EDE models. We also thank Klaus Dolag for useful discussions. Computations were performed on the OPA machine at the computer centre of the Max Planck Society. This research was supported by the DFG cluster of excellence Origin and Structure of the Universe.

REFERENCES

Bartelmann M., Doran M., Wetterich C., 2006, A&A, 454, 27
Bryan G. L., Norman M. L., 1998, ApJ, 495, 80
Bullock J. S., Kolatt T. S., Sigad Y., Somerville R. S., Kravtsov A. V., Klypin A. A., Primack J. R., Dekel A., 2001, MNRAS, 321, 559
Conroy C., Newman J. A., Davis M., Coil A. L., Yan R., Cooper M. C., Gerke B. F., Faber S. M., Koo D. C., 2005, ApJ, 635, 982
Conroy C., Prada F., Newman J. A., Croton D., Coil A. L., Conselice C. J., Cooper M. C., Davis M., Faber S. M., Gerke B. F., Guhathakurta P., Klypin A., Koo D. C., Yan R., 2007, ApJ, 654, 153
Davis M., Gerke B. F., Newman J. A., the Deep2 Team 2005, in Wolff S. C., Lauer T. R., eds, Observing Dark Energy Vol. 339 of Astronomical Society of the Pacific Conference Series, Constraining Dark Energy with the DEEP2 Redshift Survey. p. 128
De Lucia G., Kauffmann G., Springel V., White S. D. M., Lanzoni B., Stoehr F., Tormen G., Yoshida N., 2004, MNRAS, 348, 333
Dolag K., Bartelmann M., Perrotta F., Baccigalupi C., Moscardini L., Meneghetti M., Tormen G., 2004, A&A, 416, 853
Doran M., Karwan K., Wetterich C., 2005, Journal of Cosmology and Astro-Particle Physics, 11, 7
Doran M., Robbers G., Wetterich C., 2007, Phys. Rev. D, 75, 023003
Doran M., Schwindt J.-M., Wetterich C., 2001, Phys. Rev. D, 64, 123520
Efstathiou G., Frenk C. S., White S. D. M., Davis M., 1988, MNRAS, 235, 715
Eke V. R., Cole S., Frenk C. S., 1996, MNRAS, 282, 263
Eke V. R., Navarro J. F., Steinmetz M., 2001, ApJ, 554, 114
Espino-Briones N., Plionis M., Ragone-Figueroa C., 2007, ApJ, 666, L5
Evrard A. E., Bialek J., Busha M., White M., Habib S., Heitmann K., Warren M., Rasia E., Tormen G., Moscardini L., Power C., Jenkins A. R., Gao L., Frenk C. S., Springel V., White S. D. M., Diemand J., 2008, ApJ, 672, 122

Faltenbacher A., Diemand J., 2006, MNRAS, 369, 1698
Faltenbacher A., Mathews W. G., 2007, MNRAS, 375, 313
Ferreira P. G., Joyce M., 1998, Phys. Rev. D, 58, 023503
Francis M. J., Lewis G. F., Linder E. V., 2008, ArXiv e-prints, 0808.2840
Gao L., Navarro J. F., Cole S., Frenk C. S., White S. D. M., Springel V., Jenkins A., Neto A. F., 2008, MNRAS, 387, 536
Jenkins A., Frenk C. S., White S. D. M., Colberg J. M., Cole S., Evrard A. E., Couchman H. M. P., Yoshida N., 2001, MNRAS, 321, 372
Klypin A., Macciò A. V., Mainini R., Bonometto S. A., 2003, ApJ, 599, 31
Komatsu E., Dunkley J., Nolta M. R., Bennett C. L., Gold B., Hinshaw G., Jarosik N., Larson D., Limon M., Page L., Spergel D. N., Halpern M., Hill R. S., Kogut A., Meyer S. S., Tucker G. S., Weiland J. L., Wollack E., Wright E. L., 2008, ArXiv e-prints, 0803.0547
Kowalski M. e. a., 2008, ArXiv e-prints, 0804.4142
Kravtsov A. V., Klypin A. A., Khokhlov A. M., 1997, ApJS, 111, 73
Lacey C., Cole S., 1993, MNRAS, 262, 627
Lacey C., Cole S., 1994, MNRAS, 271, 676
Liddle A. R., Scherrer R. J., 1999, Phys. Rev. D, 59, 023509
Lin L., Koo D. C., Willmer C. N. A., Patton D. R., Conselice C. J., Yan R., Coil A. L., Cooper M. C., Davis M., Faber S. M., Gerke B. F., Guhathakurta P., Newman J. A., 2004, ApJ, 617, L9
Linder E. V., Jenkins A., 2003, MNRAS, 346, 573
Macciò A. V., Dutton A. A., van den Bosch F. C., 2008, ArXiv e-prints, 0805.1926
Macciò A. V., Dutton A. A., van den Bosch F. C., Moore B., Potter D., Stadel J., 2007, MNRAS, 378, 55
Macciò A. V., Quercellini C., Mainini R., Amendola L., Bonometto S. A., 2004, Phys. Rev. D, 69, 123516
Mainini R., Macciò A. V., Bonometto S. A., 2003, New Astronomy, 8, 173
Navarro J. F., Frenk C. S., White S. D. M., 1995, MNRAS, 275, 720
Navarro J. F., Frenk C. S., White S. D. M., 1996, ApJ, 462, 563
Navarro J. F., Frenk C. S., White S. D. M., 1997, ApJ, 490, 493
Neto A. F., Gao L., Bett P., Cole S., Navarro J. F., Frenk C. S., White S. D. M., Springel V., Jenkins A., 2007, MNRAS, 381, 1450
Perlmutter S. e. a., 1999, ApJ, 517, 565
Power C., Navarro J. F., Jenkins A., Frenk C. S., White S. D. M., Springel V., Stadel J., Quinn T., 2003, MNRAS, 338, 14
Press W. H., Schechter P., 1974, ApJ, 187, 425
Ratra B., Peebles P. J. E., 1988, Phys. Rev. D, 37, 3406
Riess A. G., Filippenko A. V., Li W., Treffers R. R., Schmidt B. P., Qiu Y., Hu J., Armstrong M., Faranda C., Thouvenot E., Buil C., 1999, AJ, 118, 2675
Riess A. G. e. a., 2004, ApJ, 607, 665
Sheth R. K., Mo H. J., Tormen G., 2001, MNRAS, 323, 1
Sheth R. K., Tormen G., 1999, MNRAS, 308, 119
Sheth R. K., Tormen G., 2002, MNRAS, 329, 61
Smith R. E., Peacock J. A., Jenkins A., White S. D. M., Frenk C. S., Pearce F. R., Thomas P. A., Efstathiou G., Couchman H. M. P., 2003, MNRAS, 341, 1311
Springel V., 2005, MNRAS, 364, 1105
Springel V., White S. D. M., Tormen G., Kauffmann G., 2001, MNRAS, 328, 726
Springel V., Yoshida N., White S. D. M., 2001, New Astronomy, 6, 79
Vale A., Ostriker J. P., 2004, MNRAS, 353, 189
Wang L., Steinhardt P. J., 1998, ApJ, 508, 483
Warren M. S., Abazajian K., Holz D. E., Teodoro L., 2006, ApJ, 646, 881
Wetterich C., 1988, Nuclear Physics B, 302, 668
Wetterich C., 2004, Physics Letters B, 594, 17
White S. D. M., Efstathiou G., Frenk C. S., 1993, MNRAS, 262, 1023